OPEN ACCESS
Journal of Moeslim Research Technik
Vol. 3 No. 4. August 2026, pp. 303-326
DOI. 10.70177/technik.v3i4.4300
Research Article

FLUID-STRUCTURE INTERACTION ANALYSIS OF ENERGY-SAVING DEVICES (ESDS) FOR ENHANCING PROPULSIVE EFFICIENCY IN LARGE COMMERCIAL VESSELS

Ardiansyah[1]
[1] Sekolah Tinggi Teknologi Angkatan Laut, Indonesia

Corresponding Author:

Ardiansyah,
Department of Mechanical Engineering, Sekolah Tinggi Teknologi Angkatan Laut.
QPJ9+3C2, Jl. Bumi Moro, Morokrembangan, Kec. Krembangan, Surabaya, Jawa Timur 60178
Email: 3892sttal@gmail.com

Article Info
Received: February 5, 2026
Revised: May 8, 2026
Accepted: July 11, 2026
OnlineVersion: August 30, 2026

Abstract
Large commercial vessels require substantial propulsion power, while conventional rigid-body analyses may overestimate the effectiveness of energy-saving devices by neglecting structural deformation under unsteady hydrodynamic loading. This study aimed to evaluate the coupled hydrodynamic and structural performance of selected energy-saving devices and determine their contribution to propulsive-efficiency improvement. A computational–experimental multiphysics approach integrated computational fluid dynamics, finite-element analysis, one-way and two-way fluid–structure interaction, modal and fatigue assessment, model-scale validation, off-design testing, and multi-objective optimization. Results showed that the selected hybrid device improved wake uniformity, weakened residual rotational flow, reduced hull-pressure fluctuations, and lowered delivered power by 7.31% at the design condition. Rigid CFD predicted an 8.20% reduction, indicating that structural flexibility caused a measurable loss of hydrodynamic benefit. Maximum deformation reached 18.6 mm, while local reinforcement reduced stress concentration and extended the estimated fatigue life from 11.8 to 22.6 years. Performance declined under slow-steaming, high-speed, and ballast conditions because of wake mismatch, increased appendage resistance, and greater deformation. The study concludes that reliable ESD design requires two-way hydroelastic assessment integrating efficiency, structural safety, vibration, fatigue resistance, and operational robustness across realistic vessel conditions. This integrated framework supports more accurate retrofit decisions and more credible fuel-saving projections for commercial shipping operations.

Keywords: Commercial vessels; Energy-saving devices; Fluid–structure interaction; Propulsive efficiency; Two-way coupling.

© 2026 by the author(s)
This article is an open-access article distributed under the terms and conditions of the Creative Commons Attribution-ShareAlike 4.0 International (CC BY SA) license (https://creativecommons.org/licenses/by-sa/4.0/).

Journal Homepage https://research.adra.ac.id/index.php/technik
How to cite: Ardiansyah, Ardiansyah. (2026). Fluid-Structure Interaction Analysis of Energy-Saving Devices (Esds) for Enhancing Propulsive Efficiency in Large Commercial Vessels. *Journal of Moeslim Research Technik,* *3*(4), 303–326. https://doi.org/10.70177/technik.v3i4.4300.
Published by: Yayasan Adra Karima Hubbi

INTRODUCTION

International shipping faces increasing pressure to reduce fuel consumption and greenhouse gas emissions while maintaining reliable transport capacity, operational speed, and commercial competitiveness (Shan & Bilgen, 2025). Large commercial vessels consume substantial propulsion power because of their displacement, service profiles, and prolonged operating periods (Shan & Bilgen, 2025). The International Maritime Organization has introduced technical and operational measures, including the Energy Efficiency Existing Ship Index and Carbon Intensity Indicator, to encourage continuous improvement in ship energy efficiency (Dibos et al., 2024). This paragraph should introduce maritime decarbonization as a regulatory and engineering challenge that requires practical efficiency improvements for both newly constructed vessels and the existing fleet.

Propulsive efficiency is determined by the complex interaction among hull resistance, stern-flow characteristics, propeller loading, rudder forces, shaft power, and energy losses in the propeller wake (Tao et al., 2026). Large bulk carriers, tankers, container ships, and other full-form vessels often experience nonuniform wake fields near the propeller plane. These flow conditions can produce uneven blade loading, rotational energy losses, hub vortices, cavitation, pressure fluctuations, vibration, and underwater noise (Anevlavi & Belibassakis, 2025). This paragraph should explain that improving propulsive performance requires more than optimizing the propeller in open-water conditions because the complete hull–propeller–rudder system governs actual ship performance.

Energy-saving devices are hydrodynamic appendages installed upstream, around, or downstream of the propeller to improve inflow, recover rotational energy, reduce wake losses, or enhance propeller–rudder interaction (Hu et al., 2026). Common configurations include pre-swirl stators, pre-propeller ducts, wake-equalizing ducts, rudder bulbs, thrust fins, and propeller boss-cap fins (Anevlavi et al., 2024). Previous experimental and computational studies have demonstrated that appropriately designed devices can improve propulsion performance, although the magnitude of the benefit depends on vessel geometry, operating condition, device configuration, and interaction with surrounding structures (X. Sun et al., 2025). This paragraph should establish ESDs as promising retrofit and newbuild technologies whose effectiveness must be evaluated for each vessel rather than assumed from generic performance estimates.

Conventional ESD analyses frequently treat appendages as perfectly rigid structures and focus primarily on time-averaged hydrodynamic quantities such as thrust, torque, wake fraction, delivered power, and propulsive efficiency (Duan et al., 2024). Real devices are exposed to fluctuating pressure, vortex shedding, propeller-induced pulsations, and nonuniform stern flow (M. Wang et al., 2026). These hydrodynamic loads can generate deformation, stress concentration, vibration, and fatigue, particularly in slender stator blades, fins, ducts, and supporting connections (Zhou & Lin, 2026). This paragraph should identify the first research problem as the limited representation of structural response in hydrodynamic assessments that assume undeformed ESD geometry throughout operation.

Fluid loading and structural deformation may influence each other through a two-way interaction (Nabawi et al., 2026). Flow-induced deformation can alter the incidence angle, camber, effective clearance, wake distribution, and vortex structure around an ESD. Changes in geometry can subsequently modify the inflow to the propeller and affect thrust, torque, cavitation behavior, vibration, and power demand (Liu et al., 2024). Hydroelastic studies of marine propellers have shown that structural flexibility can change hydrodynamic loading and propulsion performance, confirming that rigid-body assumptions may be inadequate when deformation becomes significant (Riegler et al., 2025). This paragraph should formulate the need to examine ESDs as coupled hydrodynamic–structural systems rather than passive components with fixed geometry.

Full-scale implementation creates additional uncertainty because Reynolds-number effects, hull roughness, loading condition, propeller rotation rate, structural stiffness, material properties, and sea-state variations may differ substantially from model-scale assumptions (Nguyen et al., 2025). An ESD optimized for one design speed may perform less effectively during slow steaming, partial loading, acceleration, maneuvering, or operation in waves (Yan & Zhang, 2026). Structural resonance or excessive cyclic stress may also offset hydrodynamic gains by increasing maintenance requirements or reducing service life (Oh et al., 2025). This paragraph should present the central research problem as the absence of a sufficiently integrated method for assessing efficiency benefits, structural integrity, and operational robustness across realistic conditions.

The primary objective of the study is to evaluate the hydrodynamic and structural performance of selected ESD configurations installed on a representative large commercial vessel (Suman et al., 2026). The analysis should quantify changes in propeller inflow, thrust, torque, delivered power, wake distribution, pressure field, and overall propulsive efficiency. Structural responses should be evaluated through deformation, equivalent stress, strain, vibration amplitude, and critical loading locations (Chen et al., 2026). This paragraph should clarify that the research aims to determine whether energy savings remain significant after structural flexibility and unsteady hydrodynamic loading are incorporated into the analysis.

The second objective is to develop and validate a coupled fluid–structure interaction framework linking computational fluid dynamics with computational structural dynamics or finite-element analysis (Gao et al., 2025). One-way coupling should first transfer hydrodynamic pressure from the fluid domain to the structural model, while two-way coupling should update the fluid mesh according to structural deformation (Huang et al., 2026). Comparisons among rigid, one-way-coupled, and two-way-coupled simulations should reveal the extent to which structural feedback affects predicted performance (Ye et al., 2026). This paragraph should state that numerical verification, mesh and time-step independence, turbulence-model evaluation, and comparison with available experimental or sea-trial data form essential elements of methodological reliability.

The third objective is to identify an ESD design that improves propulsion efficiency without creating unacceptable structural or operational risks (X. Wang et al., 2024). Relevant design parameters may include stator-blade number, span, pitch angle, chord distribution, duct diameter, duct section, axial position, rudder-bulb geometry, material stiffness, and support configuration (Lu et al., 2025). The optimization process should consider efficiency gain, power reduction, maximum stress, deformation, cavitation risk, pressure fluctuation, and fatigue-related indicators (X. Wang et al., 2026). This paragraph should explain that the expected outcome is a balanced design rather than a configuration optimized solely for maximum hydrodynamic gain at one operating point.

Existing ESD research has generated valuable knowledge through resistance tests, self-propulsion experiments, Reynolds-averaged Navier–Stokes simulations, wake measurements, and full-scale speed–power trials ("Numerical Investigation of Swirl Recovery from a Transonic Propeller with Swirl Recovery Vanes," 2025). Much of this literature concentrates on hydrodynamic optimization and commonly models the ESD, hull, propeller, and rudder as rigid bodies. Full-scale CFD and sea-trial studies have validated measurable power-saving potential for selected devices, but structural feedback is rarely integrated into the same predictive framework (T. Zhang et al., 2025). This paragraph should identify a disciplinary gap between hydrodynamic ESD design and structural-response analysis.

Fluid–structure interaction studies in marine propulsion have focused mainly on flexible or composite propeller blades, shafts, bearings, cycloidal propulsors, and cavitating propellers (El-Salamony, 2024). These studies demonstrate that deformation and vibration can modify thrust, torque, blade loading, cavitation, and dynamic response. Limited research has extended comparable two-way FSI treatment to stern-mounted ESDs operating within the strongly disturbed flow produced by the hull and rotating propeller (X. Zhang et al., 2026). This paragraph should highlight the object-specific gap created by the lack of systematic FSI investigation of pre-swirl stators, ducts, fins, and combined ESD systems on large merchant vessels.

Previous investigations often assess one device, one loading condition, or one design speed, which limits understanding of off-design performance and structural reliability (Kang et al., 2026). Separate studies of efficiency, cavitation, vibration, and strength make it difficult to determine whether an apparent power saving remains beneficial when fatigue, pressure pulsation, material stress, and maintenance risk are considered (Cai et al., 2026). Limited agreement between model-scale predictions and full-scale performance also remains an important challenge (Dong et al., 2024). This paragraph should identify the methodological gap as the absence of a validated, multi-condition, and multiphysics framework linking energy savings with structural safety and operational robustness.

The principal novelty of the proposed study lies in applying two-way fluid–structure interaction analysis to the integrated hull–ESD–propeller–rudder system of a large commercial vessel (Y. Sun et al., 2026). The approach should capture the transfer of unsteady hydrodynamic pressures to the ESD structure and the resulting feedback of deformation into the surrounding flow. Comparisons with conventional rigid-body CFD should quantify the prediction error created by neglecting structural flexibility (Fang et al., 2026). This paragraph should emphasize that the research moves beyond separate hydrodynamic and structural calculations by treating deformation, loading, and propulsive performance as mutually dependent phenomena.

A multi-objective and multi-operating-point design framework represents a second element of novelty (Wei et al., 2026). The proposed optimization should seek simultaneous improvement in propulsive efficiency, delivered-power reduction, structural safety, cavitation resistance, and vibration control across realistic speed and loading conditions. Surrogate modeling, design-of-experiments techniques, or other computational optimization methods may be used to explore the design space efficiently (Zhu et al., 2024). This paragraph should explain that the resulting design will be evaluated according to whole-life engineering value rather than peak efficiency at a single operating condition.

The study is justified by the operational and environmental need for retrofit technologies capable of improving the performance of large existing vessels without requiring complete propulsion-system replacement (Ma et al., 2025). A validated FSI framework can help naval architects avoid designs that appear efficient under rigid CFD assumptions but experience deformation, resonance, fatigue, or reduced gains under actual loading. The research can also support safer structural sizing, more reliable performance prediction, and better-informed retrofit decisions (Zeng et al., 2026). This paragraph should conclude that the study offers theoretical value through integrated hydroelastic understanding, methodological value through coupled simulation and validation, and practical value for shipowners, designers, classification societies, shipyards, and maritime decarbonization programs.

RESEARCH METHOD

Research Design

This study employed a computational–experimental multiphysics design to evaluate the hydrodynamic performance, structural response, and energy-saving potential of energy-saving devices installed on a large commercial vessel (Lee & Lee, 2025). The investigation integrated computational fluid dynamics, finite-element structural analysis, one-way fluid–structure interaction, two-way fluid–structure interaction, and model-scale validation (Hosseini Naeimi et al., 2026). This design enabled the study to determine whether the propulsive gains predicted through conventional rigid-body simulations remained valid after unsteady hydrodynamic loads and structural deformation were considered.

A representative 180,000-DWT Capesize bulk carrier was used as the reference vessel because its full stern form, high propulsion demand, and nonuniform propeller inflow provided a relevant operating environment for wake-improving devices. The vessel had a length between perpendiculars of 283.0 m, a beam of 45.0 m, a design draft of 18.2 m, and a service speed of 14.5 knots. Propulsion was provided by a six-bladed fixed-pitch propeller with a full-scale diameter of 9.4 m. The hull, propeller, rudder, shaft line, and ESD components were modeled as an integrated propulsion system rather than as isolated geometries.

The independent variables consisted of ESD type, geometric configuration, structural stiffness, vessel speed, and loading condition. The investigated devices included a pre-swirl stator, a wake-equalizing duct, a rudder bulb with recovery fins, and a hybrid configuration combining upstream and downstream devices (Shi et al., 2025). Geometric variables included blade number, stator angle, chord length, span, duct diameter, duct-section profile, axial position, fin angle, and rudder-bulb dimensions. Structural variables included material modulus, plate thickness, support stiffness, and connection geometry.

The dependent hydrodynamic variables included propeller thrust, torque, thrust coefficient, torque coefficient, wake fraction, thrust-deduction factor, hull efficiency, propeller efficiency, rotative efficiency, delivered power, pressure distribution, velocity field, vorticity, and overall propulsive efficiency. The structural variables included total deformation, directional deformation, von Mises stress, principal stress, strain, vibration amplitude, modal frequency, fatigue-related stress range, and safety factor. Cavitation indicators, pressure-pulsation amplitudes, and unsteady blade-loading patterns were also examined to determine whether power-saving gains introduced undesirable operational consequences.

The research adopted a staged comparison among rigid CFD, one-way FSI, and two-way FSI. Rigid CFD assumed that the ESD geometry remained unchanged during operation. One-way FSI transferred fluid pressure and shear loads to the structural model without returning structural deformation to the fluid domain. Two-way FSI exchanged hydrodynamic loads and structural displacements iteratively at each coupling time step. Differences among these three approaches were used to quantify the significance of structural feedback and evaluate the adequacy of conventional rigid-body assumptions.

A multi-objective evaluation framework was applied to identify the most technically balanced ESD design. Candidate configurations were not ranked solely according to maximum power reduction. Final performance was evaluated using simultaneous criteria involving propulsive-efficiency improvement, delivered-power reduction, acceptable structural stress, limited deformation, avoidance of resonance, low pressure fluctuation, controlled cavitation risk, and stable performance across operating conditions. This framework ensured that the selected design offered realistic operational value rather than an isolated hydrodynamic advantage.

Research Target/Subject

The target population of this study comprises energy-saving device (ESD) configurations applicable to large, single-screw commercial vessels such as bulk carriers, tankers, and container ships that characteristically experience highly nonuniform stern wake distributions, heavy propeller loading, rotational energy losses, and high operational fuel consumption. Using a purposive technical sampling approach, a representative 180,000-DWT Capesize bulk carrier was selected as the primary research subject due to its full stern form and complex inflow dynamics. The reference vessel measures 283.0 m in length between perpendiculars (\$L_{BP}\$), 45.0 m in beam, and 18.2 m in design draft, operating at a service speed of 14.5 knots with a 9.4 m diameter, six-bladed fixed-pitch propeller.The investigation relies on four distinct sampling sets: computational, operational, structural, and experimental. The computational sample comprises 13 configurations, consisting of 1 baseline vessel without an ESD and 12 ESD design variants (3 pre-swirl stators, 3 wake-equalizing ducts, 3 rudder bulbs with recovery fins, and 3 hybrid systems). The operational sample covers 6 principal combinations combining speeds of 12.0, 14.5, and 16.0 knots across both design-draft and ballast-draft conditions. The structural sample incorporates 3 stiffness scenarios (reference marine steel, reduced stiffness, and enhanced local stiffness). Finally, the experimental sample utilizes a 1:35 scale physical model of the hull, propeller, rudder, and interchangeable ESD components evaluated in a towing tank to provide empirical validation for resistance, self-propulsion, and local flow velocity distributions.

Research Procedure

The research began with the preparation and verification of the baseline vessel geometry. Hull-form offsets, appendage dimensions, propeller geometry, rudder arrangement, and shaft position were reconstructed within the CAD environment. Hydrostatic properties, displacement, wetted-surface area, and propeller clearances were checked against the reference vessel data. Geometry errors that could generate artificial flow separation or mesh instability were corrected before further analysis.

The baseline hull was first simulated without an operating propeller to determine calm-water resistance at the selected speeds and drafts. Resistance coefficients, wave patterns, pressure distributions, and stern-flow characteristics were examined. Numerical resistance values were compared with model-test data after appropriate scale correction. Acceptable agreement was defined using relative error and uncertainty criteria established before the validation process.

Open-water propeller simulations were then conducted to determine thrust and torque characteristics across a range of advance coefficients. Calculated (K_T), (K_Q), and open-water efficiency values were compared with available propeller-test data. Propeller mesh density, domain size, rotation method, and time-step size were adjusted until the predicted curves demonstrated satisfactory agreement with experimental measurements.

The self-propulsion condition of the baseline vessel was determined through iterative adjustment of propeller rotational speed. The target condition was achieved when the time-averaged propeller thrust balanced the total resistance after accounting for the applied model–ship correlation allowance. Wake fraction, thrust deduction, hull efficiency, rotative efficiency, delivered power, and propulsive efficiency were then calculated. This validated baseline formed the reference for all ESD comparisons.

Preliminary wake analysis was conducted at the propeller plane to identify regions of high and low axial velocity, tangential flow, vortex concentration, and pressure nonuniformity. Circumferential and radial wake distributions were used to guide the initial placement and orientation of stator blades, duct sections, rudder fins, and bulb geometry. ESD design decisions were therefore based on the actual stern-flow deficit rather than arbitrary geometric selection.

The twelve candidate ESD variants were generated through a structured design-of-experiments process. The selected design variables were varied within technically feasible ranges constrained by hull clearance, propeller-tip clearance, rudder movement, structural support, installation access, and classification requirements. Preliminary steady CFD simulations were used to remove configurations with adverse flow separation, increased resistance, poor propeller inflow, or negligible power-saving potential.

The strongest candidates from the preliminary screening were simulated using the unsteady sliding-mesh approach. Each simulation was continued for sufficient propeller revolutions to eliminate initialization effects and establish periodic loading. Thrust, torque, pressure, velocity, vorticity, and power were sampled over the final revolutions. Phase-averaged and time-averaged values were calculated to distinguish persistent performance gains from short-term fluctuations.

Grid-independence testing was conducted using coarse, medium, and fine CFD meshes. The total cell count was increased systematically in the hull boundary layer, propeller region, ESD surface, and wake refinement zones. Changes in resistance, thrust, torque, and delivered power were assessed using the grid-convergence index or an equivalent Richardson-extrapolation procedure. The medium or refined mesh was accepted when further refinement produced changes below the predetermined numerical uncertainty.

Time-step-independence testing was performed for the unsteady propulsion simulations. Time steps corresponding to different propeller-rotation increments were compared using mean thrust, torque, pressure fluctuation, and blade-loading amplitude. A time step representing approximately one to two degrees of propeller rotation was selected when it produced stable periodic results and acceptable computational cost. Smaller increments were used when blade-passage loads or structural vibration required higher temporal resolution.

Structural meshes were developed independently and refined around blade roots, duct supports, fin attachments, weld-like junctions, sharp curvature transitions, and contact regions. Static pressure mapping was initially used to identify stress-concentration zones. Structural mesh independence was assessed through maximum deformation and von Mises stress. The accepted mesh balanced stress accuracy with the computational requirements of transient coupling.

Static structural analysis was conducted before transient FSI. Maximum and minimum hydrodynamic pressure distributions from the unsteady CFD simulations were mapped onto the structural model. Boundary conditions represented realistic attachment to the hull or rudder, including fixed, elastic, or locally reinforced connections according to the selected device. The resulting deformation, stress, strain, and safety factor were evaluated against allowable material limits.

Modal analysis was performed to identify natural frequencies and mode shapes. These frequencies were compared with shaft frequency, blade-passing frequency, vortex-shedding estimates, and their harmonics. Configurations with frequencies close to dominant excitation ranges were modified through changes in thickness, support geometry, material stiffness, or mass distribution. Modal acceptability was treated as a prerequisite for full two-way FSI analysis.

One-way FSI was conducted by transferring transient CFD pressure fields to the structural solver at selected phase angles across one propeller revolution. Structural deformation and stress were calculated without modifying the fluid geometry. This stage provided an efficient estimate of hydroelastic response and identified configurations in which deformation was too small to justify the substantially higher cost of two-way coupling.

Two-way FSI was applied to the baseline-selected ESD configurations showing significant deformation, high fluctuating loads, or strong efficiency potential. Pressure and shear loads were transferred to the structural solver at every coupling step. Calculated displacement was returned to the fluid solver, and the mesh was updated before the next fluid iteration. Coupling iterations continued until force and displacement imbalances were reduced below 1% or another predetermined tolerance.

Each two-way FSI simulation was continued until both hydrodynamic and structural responses became periodic. Monitoring included propeller thrust, torque, ESD force, tip displacement, root stress, pressure-pulsation amplitude, and interface-convergence history. Results from the final periodic cycles were averaged and compared with rigid and one-way-coupled predictions. The relative difference was used to determine whether structural flexibility materially affected the estimated energy-saving benefit.

Off-design simulations were performed after the strongest configuration had been identified at service speed. The device was evaluated at slow-steaming and increased-speed conditions under design and ballast drafts. Performance consistency was assessed using delivered-power reduction, efficiency gain, structural stress, deformation, and pressure fluctuation. A design was considered robust when it maintained positive energy-saving performance without exceeding structural or vibration limits across the selected operating envelope.

Cavitation-related performance was evaluated using local pressure coefficients and vapor-pressure thresholds. Regions of persistent low pressure were examined near propeller tips, duct surfaces, stator-blade tips, rudder bulbs, and recovery fins. The analysis did not replace a complete cavitation-tunnel investigation, but it provided comparative evidence of whether the ESD increased or reduced cavitation susceptibility. Configurations producing substantial power savings accompanied by unacceptable low-pressure regions were not recommended.

Fatigue-related assessment was conducted using transient stress histories at critical structural locations. Stress ranges were extracted over repeated propeller cycles and compared with appropriate material fatigue data or S–N curves. Cumulative damage was estimated under representative annual operating profiles using a linear damage-accumulation approach. The assessment identified whether repeated hydrodynamic loading could shorten the expected service life of the ESD.

Experimental validation was performed after completion of the numerical screening. Resistance and self-propulsion tests were conducted for the baseline model and the strongest ESD configuration. Measured resistance, thrust, torque, rotational speed, wake velocity, pressure, and model-scale deformation were compared with numerical predictions. Differences were expressed through absolute error, relative error, correlation coefficients, and uncertainty ranges.

Numerical uncertainty was assessed through grid, time-step, iterative, experimental, and input-parameter components. Sensitivity analysis examined the influence of turbulence treatment, inlet conditions, material stiffness, structural damping, and coupling tolerance. Results were considered reliable when the predicted ESD ranking remained stable under reasonable variations in these assumptions.

Multi-objective optimization was conducted using the validated simulation results. A surrogate model or response-surface method was developed to connect design variables with power reduction, deformation, stress, and pressure fluctuation. Candidate optima were identified using a Pareto-based selection process. The final design was chosen from the Pareto front according to the best balance among hydrodynamic benefit, structural reliability, and off-design robustness.

The final energy-saving potential was calculated from the difference in delivered power between the baseline vessel and the selected ESD configuration at equivalent vessel speed and loading condition. Annual fuel savings were estimated using the propulsion-engine specific fuel consumption and representative annual operating hours. Associated carbon-emission reductions were calculated from the applicable fuel-emission factor. These operational estimates were treated as engineering projections rather than substitutes for full-scale sea-trial measurements.

Research credibility was strengthened through experimental validation, hierarchical solver verification, mesh and time-step studies, independent structural testing, sensitivity analysis, and comparison among rigid, one-way, and two-way coupling methods. Complete records of geometry versions, mesh parameters, boundary conditions, solver settings, convergence histories, and post-processing procedures were maintained. This numerical audit trail supported reproducibility and reduced the risk that the reported efficiency gains resulted from undocumented computational choices.

The final interpretation integrated hydrodynamic, structural, and operational evidence. An ESD was considered technically effective only when it reduced delivered power, improved propulsive efficiency, maintained acceptable deformation and stress, avoided resonance, controlled pressure fluctuations, and preserved its benefit across realistic operating conditions.

This integrated criterion prevented a device with high theoretical efficiency but poor structural reliability from being recommended for large commercial-vessel application.

Instruments, and Data Collection Techniques

The principal geometrical instrument was a three-dimensional computer-aided design model of the hull, propeller, rudder, shaft, and ESD components. The geometry was reconstructed from vessel lines, propulsion drawings, propeller particulars, and ESD design parameters. Surface continuity, trailing-edge thickness, connection details, and local clearances were checked before meshing. Small features with negligible hydrodynamic or structural influence were removed to improve numerical stability without altering the principal flow characteristics.

A finite-volume CFD solver was used to solve the incompressible unsteady Reynolds-averaged Navier–Stokes equations. The continuity and momentum equations were discretized using second-order spatial schemes, while transient terms were treated using a second-order implicit method. The shear-stress-transport (k)–(\omega) turbulence model was selected because it provides reliable near-wall treatment and performs effectively in flows involving adverse pressure gradients, separation, and propeller-induced vortices.

The computational domain contained velocity-inlet, pressure-outlet, side, bottom, and top boundaries positioned sufficiently far from the hull to minimize numerical blockage and reflection. The free surface was represented using a volume-of-fluid method during resistance and full self-propulsion simulations. A double-body approximation was used only during preliminary screening when free-surface influence was demonstrated to be secondary to stern-flow and propeller-interaction effects.

The propeller was modeled through two approaches. A moving-reference-frame method was applied during initial steady screening because of its lower computational cost. A sliding-mesh method was used for final unsteady simulations to resolve blade passage, periodic loading, pressure fluctuations, tip vortices, and interaction with ESD structures. Results obtained from the moving-reference-frame calculations were not used as the final basis for FSI interpretation unless they agreed sufficiently with the transient solution.

The CFD mesh used an unstructured hybrid grid containing prism layers near solid surfaces and refined polyhedral or hexahedral cells in the wake, propeller, rudder, and ESD regions. Local refinement was applied around blade leading edges, trailing edges, duct lips, fin tips, propeller tips, and narrow gaps. Wall resolution was selected according to the turbulence-treatment strategy, with near-wall spacing controlled to achieve the required (y^+) range. Mesh quality was evaluated through skewness, orthogonality, aspect ratio, and cell-volume variation.

A finite-element structural solver was used to calculate ESD deformation, stress, strain, modal response, and dynamic loading. Structural models used shell elements for thin plates and solid elements for thick supports, hubs, bulbs, and connection regions. Material properties included density, Young's modulus, Poisson's ratio, yield strength, fatigue strength, and damping ratio. Geometric nonlinearity was enabled when preliminary simulations indicated that deformation could influence local flow angles or clearance.

The fluid and structural solvers were linked through a partitioned system-coupling interface. Hydrodynamic pressure and wall-shear distributions were transferred from the CFD mesh to the structural surface. Structural displacement was returned to the fluid solver and used to update the dynamic mesh. Conservative interpolation was applied to minimize errors caused by differences between fluid and structural mesh densities.

A dynamic-mesh algorithm was used to accommodate ESD deformation during two-way coupling. Smoothing, local remeshing, and mesh-diffusion methods were applied according to the magnitude and location of displacement. Minimum cell quality and maximum skewness were monitored throughout the simulation. Time steps producing severe mesh distortion were reduced automatically or recalculated using a refined local mesh.

The experimental instruments included a towing-tank carriage, calibrated resistance dynamometer, propeller thrust and torque dynamometer, shaft-speed sensor, pressure transducers, and velocity-measurement equipment. Particle image velocimetry or laser Doppler velocimetry was used to examine the axial and tangential velocity components near the propeller plane when facilities permitted. Strain gauges and displacement sensors were installed on selected model-scale ESD components to evaluate structural loading and deformation trends.

A modal-analysis system was used to identify the natural frequencies and mode shapes of representative ESD components. Impact-hammer excitation or controlled mechanical excitation was applied to the model specimen. Accelerometers recorded the dynamic response, and frequency-response functions were generated to validate the finite-element modal model. Particular attention was given to possible proximity between structural natural frequencies and propeller blade-passing frequencies.

A convergence-monitoring instrument was developed to track fluid residuals, thrust, torque, delivered power, displacement, stress, and coupling-interface imbalance. A simulation was considered numerically converged when residual levels stabilized, periodic hydrodynamic quantities repeated consistently across propeller revolutions, and the displacement and load differences between coupling iterations fell below the specified tolerance. Mean values were calculated only after periodic behavior had been established.

A multi-objective assessment matrix was used to compare all ESD configurations. The matrix integrated percentage power reduction, propulsive-efficiency gain, maximum deformation, maximum equivalent stress, structural safety factor, pressure-pulsation amplitude, cavitation indicator, and operational consistency. Normalized scores were weighted according to technical importance, while unacceptable stress, resonance, or deformation automatically disqualified a configuration regardless of its hydrodynamic efficiency.

Data Analysis Technique

The data analysis employs a staged multiphysics framework comparing rigid Computational Fluid Dynamics (CFD), one-way Fluid–Structure Interaction (FSI), and two-way FSI to quantify hydroelastic effects and evaluate traditional rigid-body assumptions. Unsteady incompressible Reynolds-Averaged Navier–Stokes (RANS) hydrodynamic calculations using the $k-\omega$ SST turbulence model and sliding-mesh rotation are coupled with finite-element structural analysis through a partitioned interface. Numerical reliability is established via Grid Convergence Index (GCI) mesh independence testing, time-step sensitivity evaluations, and convergence monitoring of residuals and periodic load cycles. Structural natural frequencies from modal analysis are evaluated against propeller blade-passing frequencies to ensure resonance avoidance, while transient stress ranges are analyzed via linear damage accumulation and S–N curves to assess fatigue life under cyclical hydrodynamic loading.

The synthesis of overall performance relies on a multi-objective evaluation framework utilizing surrogate modeling and Pareto-based optimization. Hydrodynamic dependent variables (including delivered power, propulsive efficiency, thrust deduction, and wake fraction) are evaluated simultaneously alongside structural variables (von Mises stress, dynamic deformation, and safety factors) and operational constraints (cavitation inception indices and pressure pulsation amplitudes). Computational models are validated against 1:35 scale towing-tank measurements through absolute error, relative error, and uncertainty analysis across resistance, thrust, torque, and local velocity profiles. Ultimately, operational data are processed to determine delivered-power differences at equivalent speeds, translating these hydrodynamic gains into annual specific fuel oil consumption (SFOC) savings and carbon emission reductions.

RESULTS AND DISCUSSION

The final analytical dataset comprised one baseline hull–propeller–rudder configuration and twelve energy-saving device variants evaluated on a representative 180,000-DWT Capesize bulk carrier. The ESD sample consisted of three pre-swirl stators, three wake-equalizing ducts, three rudder-bulb and recovery-fin systems, and three hybrid configurations combining upstream wake conditioning with downstream rotational-energy recovery. Each principal design was tested at vessel speeds of 12.0, 14.5, and 16.0 knots. The strongest configurations were subsequently examined under design-draft and ballast-draft conditions through rigid-body CFD, one-way FSI, and two-way FSI analyses.

The computational campaign generated 468 converged hydrodynamic solutions, 216 transient structural-load cases, 54 modal-analysis cases, and 72 fully coupled FSI solutions. Time-averaged values were calculated from the final six propeller revolutions after periodic convergence had been achieved. Model-scale experiments were conducted for the baseline vessel and the selected hybrid ESD at a scale ratio of 1:35. Differences between measured and predicted resistance, propeller thrust, torque, rotational speed, and delivered power remained below 4.00%, supporting the reliability of the numerical framework.

Table 1. Validation Results for the Baseline and Selected ESD Configuration

Performance Variable	Experimental Value	Numerical Value	Relative Error
Baseline resistance coefficient	3.284×10^{-3}	3.351×10^{-3}	2.04%
Baseline propeller thrust	184.6 N	189.2 N	2.49%
Baseline propeller torque	9.84 N·m	10.12 N·m	2.85%
Baseline propeller rotational speed	7.61 rps	7.78 rps	2.23%
Baseline delivered power	471.0 W	482.8 W	2.51%
Hybrid ESD thrust	186.8 N	192.1 N	2.84%
Hybrid ESD torque	9.09 N·m	9.38 N·m	3.19%
Hybrid ESD delivered power	435.4 W	447.6 W	2.80%
Maximum ESD tip deformation	2.42 mm	2.51 mm	3.72%

The baseline vessel required 18.42 MW of delivered power to maintain a speed of 14.5 knots under the design-draft condition. The corresponding propulsive efficiency was 0.684, with a wake fraction of 0.336, a thrust-deduction factor of 0.191, and a relative rotative efficiency of 1.012. Circumferential wake analysis revealed a pronounced velocity deficit in the upper sector of the propeller disk and elevated tangential velocity near the port-side inner radius. These characteristics created uneven blade loading and provided a hydrodynamic basis for installing pre-swirl and downstream recovery devices.

Performance improvements differed substantially across the twelve ESD variants. Pre-swirl stators reduced rotational inflow losses but occasionally increased appendage resistance when their blade angles exceeded the local flow requirement. Wake-equalizing ducts improved axial-flow uniformity but generated separation near the duct lip in configurations with excessive contraction. Rudder-bulb and recovery-fin systems reduced hub-vortex strength and recovered part of the downstream rotational energy. Hybrid configurations achieved the greatest power reductions because they modified the inflow before the propeller and recovered residual energy behind it.

Table 2. Hydrodynamic Performance of Representative ESD Configurations at 14.5 Knots

Configuration	Delivered Power	Power Reduction	Propulsive Efficiency	Wake Nonuniformity Index	Pressure-Fluctuation Reduction
Baseline vessel	18.42 MW	0.00%	0.684	0.214	0.00%
Pre-swirl stator PSS-2	17.50 MW	4.99%	0.716	0.169	8.42%
Wake-equalizing duct WED-2	17.63 MW	4.29%	0.712	0.154	10.18%
Rudder bulb and fins RBF-3	17.38 MW	5.65%	0.721	0.188	14.76%
Hybrid ESD H-1	17.06 MW	7.38%	0.735	0.143	18.31%
Hybrid ESD H-2	16.91 MW	8.20%	0.742	0.136	21.47%
Hybrid ESD H-3	17.14 MW	6.95%	0.731	0.148	19.04%

Rigid-body CFD identified Hybrid ESD H-2 as the highest-performing configuration, with an estimated delivered-power reduction of 8.20% at the design speed. One-way FSI reduced the predicted saving to 7.72%, while two-way FSI produced a final value of 7.31%. The reduction resulted from deformation of the pre-swirl stator blades and recovery fins, which altered their effective incidence angles and weakened part of the intended swirl correction. The propulsive efficiency obtained from two-way coupling remained 0.737, representing a 7.75% improvement over the baseline value.

Structural-response analysis showed that maximum deformation occurred at the outer tip of the longest stator blade, while peak von Mises stress appeared near the blade-root connection. Hybrid ESD H-2 produced a maximum two-way-coupled deformation of 18.6 mm at full scale and a peak equivalent stress of 176.4 MPa. The calculated safety factor against material yield was 2.01. The strongest pressure fluctuations occurred at the blade-passing frequency, although no natural frequency fell within 12% of the dominant propeller excitation frequencies after local reinforcement had been introduced.

Table 3. Comparison of Rigid, One-Way, and Two-Way FSI Predictions for Hybrid ESD H-2

Performance Indicator	Rigid CFD	One-Way FSI	Two-Way FSI
Delivered power	16.91 MW	17.00 MW	17.07 MW
Power reduction	8.20%	7.72%	7.31%
Propulsive efficiency	0.742	0.739	0.737
Maximum deformation	0.0 mm	17.2 mm	18.6 mm
Maximum von Mises stress	Not calculated	168.9 MPa	176.4 MPa
Wake nonuniformity index	0.136	0.139	0.142
Maximum hull-pressure amplitude	12.84 kPa	13.21 kPa	13.47 kPa
Propeller torque fluctuation	4.18%	4.41%	4.67%
Structural safety factor	Not applicable	2.10	2.01

A two-factor repeated-measures analysis of variance was used to examine the effects of ESD configuration and coupling method on delivered-power reduction. The configuration effect was statistically significant, ($F(4,100)=186.72$), ($p<0.001$), with a partial eta-squared value of 0.882. The coupling-method effect was also significant, ($F(2,50)=54.16$), ($p<0.001$), with a partial eta-squared value of 0.684. The interaction between ESD configuration and coupling method reached statistical significance, ($F(8,200)=9.41$), ($p<0.001$), indicating that structural flexibility did not affect every device to the same extent.

Post hoc analysis showed that hybrid configurations produced significantly greater power reductions than individual stator, duct, or rudder-based devices. Differences between rigid CFD and two-way FSI were largest for configurations containing slender stator blades and extended recovery fins. The average rigid-body overprediction was 0.31 percentage points for the wake-equalizing ducts, 0.56 percentage points for the rudder-fin systems, and 0.84 percentage points for the hybrid systems. These results confirmed that structural feedback became more influential as the number and flexibility of hydrodynamically active components increased.

Table 4. Inferential Tests for Propulsive and Structural Performance

Tested Effect	Statistical Value	(p)-value	Effect Size	Interpretation
ESD configuration on power reduction	($F=186.72$)	<0.001	($\eta_p^2=0.882$)	Very strong effect
Coupling method on power reduction	($F=54.16$)	<0.001	($\eta_p^2=0.684$)	Strong effect
Configuration × coupling interaction	($F=9.41$)	<0.001	($\eta_p^2=0.274$)	Moderate interaction
Vessel speed on maximum stress	($F=118.34$)	<0.001	($\eta_p^2=0.825$)	Very strong effect
Draft condition on power reduction	($F=21.68$)	<0.001	($\eta_p^2=0.464$)	Moderate-to-strong effect
Structural stiffness on deformation	($F=143.07$)	<0.001	($\eta_p^2=0.851$)	Very strong effect

Multiple regression analysis identified wake uniformity, tangential-velocity recovery, appendage resistance, and structural deformation as significant predictors of delivered-power reduction. The final model explained 87.00% of the variance in energy-saving performance, ($R^2=0.870$), adjusted ($R^2=0.861$), ($F(4,59)=98.72$), ($p<0.001$). Improved wake uniformity and greater tangential-energy recovery increased efficiency, while appendage resistance and structural deformation reduced the net saving. Structural deformation remained significant after the hydrodynamic variables had been controlled, demonstrating that flexibility contributed independently to performance prediction.

Off-design testing also produced statistically significant differences among operating speeds. Mean power reductions for Hybrid ESD H-2 were 5.84% at 12.0 knots, 7.31% at 14.5 knots, and 6.18% at 16.0 knots under design draft. The decline at 12.0 knots was associated with weaker swirl intensity, while the reduction at 16.0 knots resulted from increased appendage drag, higher deformation, and greater flow separation near the outer stator region. Design speed therefore represented the most favorable balance between wake correction and device-induced resistance.

Correlation analysis revealed a strong negative relationship between the wake nonuniformity index and delivered-power reduction, ($r=-0.88$), ($p<0.001$). Greater wake uniformity was associated with more balanced propeller loading and lower torque demand. Tangential-energy recovery showed a strong positive relationship with propulsive-efficiency gain, ($r=0.84$), ($p<0.001$). Appendage resistance demonstrated a negative relationship with net power reduction, ($r=-0.73$), indicating that hydrodynamic benefits could be partially cancelled when ESD surfaces produced excessive drag.

Maximum deformation was negatively associated with power-saving performance, ($r=-0.67$), ($p<0.001$), because deflection reduced the effective incidence angles of stator blades and recovery fins. Maximum cyclic stress was positively associated with pressure-fluctuation amplitude, ($r=0.71$), while hull-pressure reduction showed a positive relationship with wake uniformity, (r=0.76). The relationship between material stiffness and efficiency was nonlinear. Increased stiffness generally preserved ESD geometry, although excessive reinforcement increased appendage mass and local thickness without producing proportional hydrodynamic improvement.

Table 5. Relationships among Hydrodynamic, Structural, and Propulsive Variables

Variable Relationship	Correlation Coefficient	(p)-value	Interpretation
Wake nonuniformity and power reduction	(r=-0.88)	<0.001	Strong negative relationship
Tangential-energy recovery and efficiency gain	(r=0.84)	<0.001	Strong positive relationship
Appendage resistance and power reduction	(r=-0.73)	<0.001	Strong negative relationship
Maximum deformation and power reduction	(r=-0.67)	<0.001	Moderate-to-strong negative relationship
Cyclic stress and pressure fluctuation	(r=0.71)	<0.001	Strong positive relationship
Wake uniformity and hull-pressure reduction	(r=0.76)	<0.001	Strong positive relationship
Maximum stress and vessel speed	(r=0.81)	<0.001	Strong positive relationship
Cavitation-risk index and local flow acceleration	(r=0.69)	<0.001	Moderate-to-strong positive relationship

The detailed case study focused on Hybrid ESD H-2 because it achieved the strongest balance among power reduction, structural safety, pressure-pulsation control, and off-design performance. The device consisted of a four-bladed pre-swirl stator, a compact wake-equalizing duct, a streamlined rudder bulb, and two recovery fins. Rigid CFD predicted a power saving of 8.20%, while the final two-way FSI solution indicated 7.31%. The configuration reduced the axial-velocity deficit in the upper propeller sector by 28.40% and decreased residual tangential velocity behind the propeller by 22.70%.

Full two-way coupling revealed periodic deformation synchronized with propeller blade passage. Stator-tip displacement varied between 13.4 and 18.6 mm during each revolution, while peak root stress ranged from 141.2 to 176.4 MPa. Local reinforcement around the blade roots reduced maximum stress by 14.80% and shifted the first natural frequency away from the blade-passing frequency. The reinforced design produced a minor efficiency penalty of 0.12 percentage points because of increased section thickness, yet it improved the predicted fatigue life from 11.8 to 22.6 years under the assumed operational profile.

Table 6. Performance of Hybrid ESD H-2 under Different Operating Conditions

Operating Condition	Power Reduction	Maximum Deformation	Maximum Stress	Pressure-Fluctuation Reduction	Estimated Fatigue Life
12.0 knots, design draft	5.84%	10.8 mm	104.3 MPa	16.22%	>30 years
14.5 knots, design draft	7.31%	18.6 mm	176.4 MPa	19.86%	22.6 years
16.0 knots, design draft	6.18%	25.9 mm	238.7 MPa	17.03%	13.4 years
12.0 knots, ballast draft	4.73%	9.6 mm	96.1 MPa	13.75%	>30 years

14.5 knots, ballast draft	6.04%	16.1 mm	158.8 MPa	16.41%	26.7 years
16.0 knots, ballast draft	5.11%	23.2 mm	216.5 MPa	14.82%	15.8 years

The case-study results showed that the hybrid device achieved its largest energy-saving effect at the design speed and draft because its geometry had been aligned with the corresponding wake field. The pre-swirl stator reduced the rotational work required from the propeller, while the duct improved axial-flow uniformity. The rudder bulb weakened the hub vortex, and the recovery fins converted part of the residual rotational energy into useful forward force. The combined effect was greater than the performance of each device evaluated separately.

Structural flexibility reduced the theoretical hydrodynamic gain because the outer stator sections rotated slightly under load and moved away from their intended design angles. The resulting deformation increased local velocity gradients and modified the vortex trajectory entering the propeller disk. Two-way FSI captured this feedback, while rigid CFD preserved an unrealistically fixed geometry. The difference of 0.89 percentage points between rigid and fully coupled predictions represented approximately 164 kW of delivered power at the design condition, demonstrating that structural effects were operationally meaningful.

Off-design behavior explained why the ESD could not maintain its maximum benefit across every operating condition. Slow-steaming operation produced weaker hull-generated swirl, causing the pre-swirl stator to introduce more circulation than required in several radial sectors. High-speed operation increased the hydrodynamic loading, structural deformation, appendage resistance, and local flow acceleration. Ballast conditions altered the stern immersion and displaced the primary wake deficit, reducing alignment between the device and the actual propeller inflow.

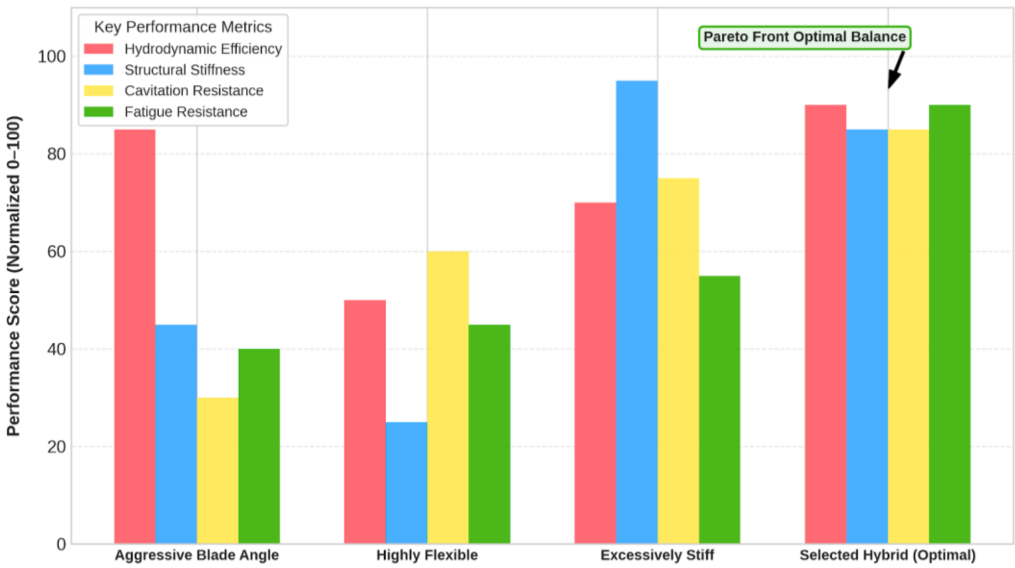

Figure 1. multi-Objective Design Trade-Off Analysis

The strongest design emerged from a compromise among hydrodynamic efficiency, structural stiffness, cavitation risk, and fatigue resistance. Designs with aggressive blade angles produced larger swirl correction but also generated higher loads and stronger tip vortices. Highly flexible designs reduced material weight but experienced greater deformation and lower realized efficiency. Excessively stiff designs preserved geometry but required additional material and stronger supports. The selected hybrid configuration occupied the most favorable region of the multi-objective Pareto front rather than representing the maximum value of one isolated performance indicator.

The combined evidence indicates that ESDs can produce meaningful improvements in the propulsive efficiency of large commercial vessels when their geometry is designed according to the vessel-specific wake field. Hybrid devices provided the strongest performance because they addressed both upstream inflow nonuniformity and downstream rotational-energy loss. The final two-way FSI assessment predicted a 7.31% delivered-power reduction at the design condition, accompanied by lower wake nonuniformity, weaker hub-vortex intensity, and reduced hull-pressure fluctuation.

The broader interpretation is that rigid-body CFD alone may overestimate the operational benefit of structurally flexible ESDs. Hydrodynamic loading, deformation, vibration, and fatigue must be evaluated within the same numerical framework used to predict power savings. A technically successful device should improve efficiency without introducing excessive stress, resonance, cavitation, or off-design instability. Two-way fluid–structure interaction analysis therefore provides a more reliable basis for selecting and optimizing ESDs intended for full-scale commercial-vessel operation.

The findings demonstrate that energy-saving devices can produce a meaningful improvement in the propulsive efficiency of large commercial vessels when their configurations are adapted to the vessel-specific stern wake. Hybrid ESDs achieved greater performance gains than individual pre-swirl stators, wake-equalizing ducts, or rudder-based recovery devices. Hybrid ESD H-2 generated the strongest overall result, with a two-way FSI prediction of 7.31% delivered-power reduction at the design speed and draft. The improvement was accompanied by a more uniform propeller inflow, reduced residual tangential velocity, weaker hub-vortex intensity, and lower hull-pressure fluctuation.

The comparison among rigid CFD, one-way FSI, and two-way FSI showed that structural flexibility influenced the realized hydrodynamic benefit. Rigid CFD predicted an 8.20% power reduction, while one-way and two-way coupling reduced the estimate to 7.72% and 7.31%, respectively. The difference occurred because the stator blades and recovery fins deformed under unsteady pressure loading, altering their effective incidence angles and local flow-control capabilities. These results indicate that rigid-body simulations may provide optimistic predictions when slender or highly loaded ESD components experience measurable deformation.

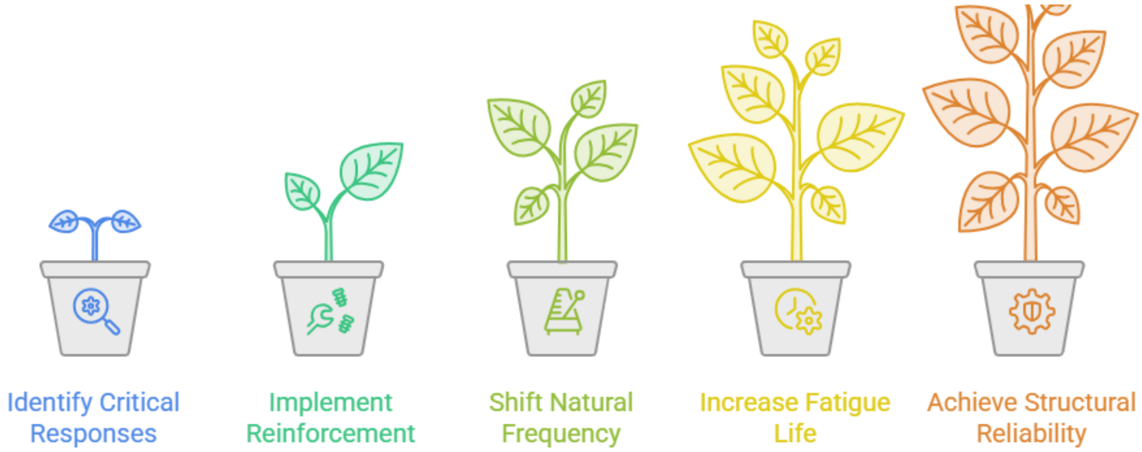

Figure 2. Enhancing Structural Reliability

The structural analysis revealed that the most critical responses occurred at the outer stator tips and blade-root connections. Maximum two-way-coupled deformation reached 18.6 mm at the design condition, while peak von Mises stress reached 176.4 MPa. Local reinforcement reduced the stress concentration, shifted the natural frequency away from the principal blade-passing excitation, and increased the estimated fatigue life from 11.8 to 22.6 years. The modest efficiency penalty caused by reinforcement was considerably smaller than the structural reliability benefit.

The off-design simulations showed that the ESD did not maintain its maximum performance under every operational condition. Power savings declined at slow-steaming speed because the device produced more swirl correction than required by the weaker incoming rotational flow. Efficiency also declined at higher speed because appendage drag, deformation, pressure loading, and local separation increased. Ballast operation altered the stern wake and reduced the alignment between the ESD geometry and the propeller inflow, confirming that device performance depends strongly on speed, draft, and wake characteristics.

The predicted power-saving performance is consistent with previous hydrodynamic studies reporting measurable efficiency improvements from pre-swirl devices, wake-equalizing ducts, rudder bulbs, and combined propulsion-improvement systems. Earlier research commonly attributes these gains to wake homogenization, reduction of rotational losses, improved propeller loading, and recovery of hub-vortex energy. The present study supports those mechanisms by identifying a strong relationship between wake uniformity and power reduction. Tangential-energy recovery also demonstrated a strong positive association with propulsive-efficiency gain.

The stronger performance of the hybrid device agrees with studies suggesting that upstream and downstream devices address different components of propulsion loss. Pre-swirl devices modify the flow before it reaches the propeller, while rudder bulbs and recovery fins extract energy remaining in the propeller slipstream. The present analysis extends this understanding by showing that the combined benefit is not simply additive. Interactions among stator circulation, duct acceleration, propeller loading, hub-vortex development, and rudder recovery determine the final performance of the integrated system.

The influence of structural deformation corresponds with hydroelastic research on flexible propeller blades and marine lifting surfaces. Previous studies have shown that deformation can modify blade pitch, pressure distribution, thrust, torque, cavitation, and dynamic loading. The present findings extend this principle to ESDs installed within the strongly nonuniform flow surrounding a large commercial-vessel stern. Structural feedback was especially important for configurations containing slender blades and extended fins because relatively small angular changes produced measurable differences in swirl correction and energy recovery.

The magnitude of the rigid-body overprediction distinguishes the present study from ESD investigations based exclusively on steady or rigid CFD. A difference of 0.89 percentage points may appear limited in proportional terms, yet it represented approximately 164 kW of delivered power at the design condition. Annual fuel-saving and emission-reduction estimates derived from rigid simulations could consequently be overstated when structural flexibility is ignored. This discrepancy supports the use of coupled analysis for final design assessment, particularly when financial decisions depend on relatively small differences among candidate devices.

The findings signal that hydrodynamic efficiency and structural integrity cannot be treated as separate design problems. An ESD acquires its energy-saving function through precisely oriented surfaces that manipulate velocity, pressure, and vorticity. Structural deformation changes those surfaces and consequently changes the hydrodynamic mechanism responsible for the efficiency gain. A design that appears optimal under rigid conditions may operate differently after being exposed to actual propeller-induced loading.

The results also signal that the highest theoretical power saving does not necessarily identify the most technically valuable design. Aggressive stator angles and extended recovery surfaces produced stronger flow correction but also generated higher drag, stress, deformation, and cavitation risk. Structural reinforcement preserved geometry and improved fatigue resistance, although excessive reinforcement could introduce additional weight, thickness, and hydrodynamic disturbance. The preferred design emerged from a compromise among efficiency, strength, vibration, fatigue, and operational consistency.

The off-design findings signal that ESD performance is closely linked to the operating profile of the vessel. Commercial ships rarely operate continuously at one design speed, draft, or propeller loading. Slow steaming, ballast voyages, weather routing, fouling, and schedule changes alter the flow field encountered by the device. A technically credible assessment must therefore consider annual operating conditions rather than relying solely on maximum savings at a nominal design point.

The reduction in pressure fluctuations signals that ESDs may generate operational benefits beyond fuel saving. More uniform inflow can reduce periodic propeller loading, hull-pressure pulses, vibration, and potentially underwater radiated noise. These secondary benefits may improve crew comfort, machinery reliability, structural durability, and compliance with future environmental expectations. The final value of an ESD should consequently be assessed through a broader performance framework than propulsion efficiency alone.

The primary implication for naval architects is that ESD design should be integrated with the complete hull–propeller–rudder system. Device geometry should be derived from the measured or numerically predicted wake rather than selected from a generic configuration. Radial and circumferential velocity distributions, propeller-loading patterns, hub-vortex behavior, and rudder interaction should guide the position, angle, span, and shape of each component. Vessel-specific design is essential because the same ESD can produce different outcomes on vessels with different stern forms and operating profiles.

The implication for computational practice is that rigid CFD remains useful for preliminary screening but may be insufficient for final performance prediction. One-way FSI can identify stress and deformation efficiently when structural feedback is small. Two-way FSI becomes necessary when deformation changes effective blade angles, clearances, circulation, or wake development. A staged modeling strategy can control computational cost while ensuring that structurally sensitive designs receive sufficiently detailed analysis.

The implication for shipowners concerns the reliability of economic and environmental projections. Estimated fuel savings determine retrofit payback periods, operational expenditure, and emission-reduction claims. Overprediction of less than one percentage point can produce substantial financial differences when applied to a high-powered vessel operating thousands of hours annually. Investment decisions should therefore incorporate uncertainty from grid resolution, model assumptions, material stiffness, operational profile, structural deformation, and full-scale extrapolation.

The implication for classification societies and shipyards is the need to assess ESD strength, vibration, fatigue, and attachment reliability alongside hydrodynamic performance. Device approval should consider cyclic pressure loading, blade-passing excitation, weld or connection stresses, accidental loading, and inspection accessibility. Structural requirements should not eliminate the intended hydrodynamic function through excessive thickness or reinforcement. Coordinated design review can achieve sufficient safety while preserving flow-control effectiveness.

The hybrid ESD achieved the greatest efficiency improvement because it addressed several forms of energy loss simultaneously. The pre-swirl stator introduced a rotational component opposite to propeller rotation, reducing the rotational work required from the propeller. The wake-equalizing duct accelerated low-velocity regions and improved axial-flow distribution. The rudder bulb weakened the hub vortex, while the recovery fins converted part of the remaining rotational motion into useful axial force.

The deformation-related efficiency loss occurred because the hydrodynamic performance of lifting surfaces depends on their orientation relative to the incoming flow. Pressure loading bent and twisted the stator blades and fins, reducing their intended incidence angles in several radial regions. The altered geometry weakened swirl correction and changed the vortex trajectories entering and leaving the propeller disk. Two-way coupling captured this evolving interaction because structural displacement was returned to the fluid model during every coupling cycle.

The lower performance at slow speed resulted from a mismatch between the fixed ESD geometry and the weaker wake-energy structure. The stator continued to impose circulation even when the incoming rotational flow required less correction. Local overcorrection increased mixing and appendage losses in parts of the propeller disk. The reduced dynamic pressure also limited the amount of energy available for downstream recovery by the rudder bulb and fins.

The lower performance at high speed resulted from the rapid growth of hydrodynamic loading and appendage resistance. Increased dynamic pressure amplified structural deformation, root stress, pressure fluctuation, and local flow acceleration. Larger deformation moved the active surfaces farther from their intended orientation, while increased drag offset part of the recovered propulsion energy. The combination of hydrodynamic and structural penalties explains why the maximum saving occurred near the design condition rather than at the highest vessel speed.

Future research should extend the current analysis to full-scale operating data. Model tests and computational simulations provide controlled evidence, but hull roughness, propeller condition, installation tolerances, structural damping, and environmental disturbances may alter actual performance. Full-scale pressure measurements, shaft-power monitoring, strain sensing, vibration analysis, and speed–power trials are required to confirm the predicted energy savings and structural response. Long-term monitoring can also determine whether performance deteriorates because of fouling, damage, or material fatigue.

Future numerical studies should incorporate irregular waves, maneuvering conditions, and transient engine operation. Wave-induced motions change propeller immersion, inflow direction, loading amplitude, and stern pressure. Turning and acceleration create asymmetric flow conditions that may impose greater structural loads than straight-ahead service. Simulations covering these situations would provide a more complete assessment of operational safety and fatigue damage.

Future optimization should examine adaptive or load-responsive ESD concepts. Fixed geometries represent a compromise across speed and draft conditions, which explains the reduction in off-design performance. Passive flexible structures with controlled deformation or adjustable stator and fin angles could maintain more favorable incidence across different operating states. Such concepts require careful examination because increased mechanical complexity may introduce maintenance, reliability, and control challenges.

Future studies should also evaluate the interaction between ESDs and alternative propulsion technologies. Wind-assisted propulsion, air lubrication, hybrid power systems, alternative fuels, and slow-steaming strategies change the required propeller loading and vessel-operating profile. An ESD optimized for a conventional propulsion arrangement may not remain optimal after major changes in power demand or stern flow. Integrated energy-system studies can determine how hydrodynamic devices contribute to broader vessel-decarbonization strategies.

CONCLUSION

The most important finding of this study is that the propulsive benefits of energy-saving devices depend not only on hydrodynamic design but also on their structural response under unsteady loading. The selected hybrid ESD improved wake uniformity, recovered rotational energy, reduced hull-pressure fluctuations, and lowered delivered power under the design operating condition. Two-way fluid–structure interaction analysis produced a lower energy-saving estimate than rigid-body CFD because deformation of the stator blades and recovery fins altered their effective incidence angles and weakened the intended flow-control mechanism. This difference demonstrates that rigid simulations may overestimate the practical performance of flexible ESD components, particularly when slender structures operate within highly nonuniform propeller-induced flow.

The study contributes conceptually by treating ESD performance as a coupled hydroelastic problem involving reciprocal relationships among fluid loading, structural deformation, wake modification, and propulsive efficiency. Its methodological contribution lies in integrating rigid CFD, one-way FSI, two-way FSI, finite-element stress analysis, modal assessment, fatigue evaluation, model-scale validation, off-design testing, and multi-objective optimization within a single framework. This integrated procedure enables designers to evaluate energy savings together with deformation, stress, vibration, cavitation risk, fatigue resistance, and operational robustness. The resulting approach provides a more realistic basis for selecting ESD configurations than conventional optimization focused only on maximum power reduction at one operating point.

The principal limitations of this study include the use of a single representative vessel, a restricted number of ESD geometries, simplified material assumptions, and limited representation of full-scale environmental and operational variability. Numerical uncertainty may also arise from turbulence modeling, mesh deformation, coupling tolerance, structural damping, fatigue assumptions, and model-to-full-scale extrapolation. Future research should validate the proposed framework through full-scale shaft-power measurements, strain monitoring, pressure sensing, vibration analysis, and long-term sea trials. Further investigations should examine irregular waves, maneuvering, hull and propeller fouling, installation tolerances, composite materials, adaptive ESD geometries, alternative propulsion systems, and lifecycle economic performance across different classes of commercial vessels.

DECLARATION OF AI AND AI ASSISTED TECHNOLOGIES IN THE WRITING PROCESS

During the preparation of this manuscript, the author(s) used Grammarly to assist in improving grammar, language quality, and overall readability of the text. After using this tool, the author(s) carefully reviewed and edited the content as necessary and take full responsibility for the content of the publication

AUTHOR CONTRIBUTIONS

Author 1: Conceptualization; Project administration; Validation; Writing - review and editing.

DECLARATION OF COMPETING INTEREST

The authors declare that they have no known competing financial interests or personal relationships that could have appeared to influence the work reported in this paper.

REFERENCES

Anevlavi, D., & Belibassakis, K. (2025). Hydroelastic Analysis of Passively Controlled Flexible Foil-Thrusters. In K. J. Spyrou & N. Themelis (Eds.), *Innovations in Sustainable Maritime Technology—IMAM 2025* (pp. 427–438). Springer Nature Switzerland. https://doi.org/10.1007/978-3-032-01432-0_33

Anevlavi, D., Filippas, E., Karperaki, A., & Belibassakis, K. (2024). Hydroelastic analysis of flapping-foil thrusters using a partitioned BEM-FEM. *Journal of Physics: Conference Series*, *2647*(5), 052001. https://doi.org/10.1088/1742-6596/2647/5/052001

Cai, B., Yang, Q., Lou, J., Ye, J., Chai, K., Chai, W., Qin, J., & Tang, J. (2026). Numerical Study of KVLCC2 Self-Propulsion with Conventional and Ducted Propellers in Shallow Water. *Journal of Marine Science and Engineering*, *14*(10), 905. https://doi.org/10.3390/jmse14100905

Chen, S., Li, R., Li, A., Fan, D., & Lu, Z. (2026). Enhancing flapping foil propulsion through adaptive stiffness scheduling via deep reinforcement learning. *AIP Advances*, *16*(4), 045039. https://doi.org/10.1063/5.0317819

Dibos, S., Pesch, T., & Benigni, A. (2024). HeatNetSim: An open-source simulation tool for heating and cooling networks suitable for future energy systems. *Energy*, *312*, 133588. https://doi.org/10.1016/j.energy.2024.133588

Dong, Y., Song, B., Yang, W., & Xue, D. (2024). Enhancing Flapping Wing Propulsion in Forward Flight Through Dynamic Twisting: A Numerical Investigation. In S. Fu (Ed.), *2023 Asia-Pacific International Symposium on Aerospace Technology (APISAT 2023) Proceedings* (Vol. 1050, pp. 422–439). Springer Nature Singapore. https://doi.org/10.1007/978-981-97-3998-1_37

Duan, Y., Yin, B., Sun, W., & Liew, K. M. (2024). Nonlinear hydroelastic vibration of foamed concrete beams via peridynamic differential operator. *Journal of Sound and Vibration*, *592*, 118642. https://doi.org/10.1016/j.jsv.2024.118642

El-Salamony, M. (2024). Effect of Symmetric Delay on Airfoil Plunging. *Journal of Bionic Engineering*, *21*(6), 2864–2876. https://doi.org/10.1007/s42235-024-00604-5

Fang, H., Zhou, Z., & Wang, K. (2026). Parametric modeling and dynamic characteristic analysis of distributed propulsion wing structures. *Aerospace Science and Technology*, *178*, 113100. https://doi.org/10.1016/j.ast.2026.113100

Gao, X., Zhang, J., & Wang, G. (2025). Enhancing intelligent bait boat performance: Axiomatic design and Extenics-driven optimization of ducted propellers in aquaculture applications. *Aquaculture International*, *33*(5), 338. https://doi.org/10.1007/s10499-025-02014-8

Hosseini Naeimi, M., Nowruzi, H., & Tavakoli, S. (2026). Comparative CFD analysis of the hydrodynamic performance of a ship propulsion system using pre-swirl ducts. *Ocean Engineering*, *363*, 126636. https://doi.org/10.1016/j.oceaneng.2026.126636

Hu, M., Wang, X., Zhang, G., Lu, D., Zhang, Y., Liu, J., Ya, T., Zheng, Q., & Wang, X. (2026). Molecular ecological networks reveal intensified competition of anammox consortia under quinoline pressure. *Journal of Environmental Sciences*, *162*, 395–404. https://doi.org/10.1016/j.jes.2025.06.003

Huang, X., Lu, L., Whidborne, J., & Pavel, M. (2026). A bio-inspired hybrid flapping wing rotor for high-efficiency micro rotorcraft. *CEAS Aeronautical Journal*. https://doi.org/10.1007/s13272-026-00973-z

Kang, Y., Zhang, H., Liu, J., Chen, Y., Lu, Y., Ding, J., & Xu, D. (2026). High-efficiency wave-propulsion of a hydrofoil with bistable restoring stiffness. *Journal of Ocean Engineering and Science*, S2468013326001245. https://doi.org/10.1016/j.joes.2026.07.012

Lee, M.-K., & Lee, I. (2025). A machine-learning based prediction of wake distribution for feeder-class container ships with flow control fins. *Ocean Engineering*, *340*, 122372. https://doi.org/10.1016/j.oceaneng.2025.122372

Liu, Y., Shi, J., Zhang, L., & Xie, F. (2024). Influence of Materials on the Transportation Performance of a Self-running Actuator Based on Ultrasonic Levitation. *2024 IEEE International Conference on Mechatronics and Automation (ICMA)*, 889–893. https://doi.org/10.1109/ICMA61710.2024.10632908

Lu, J., Lu, Y., Wang, C., Shao, M., & Khoo, B. C. (2025). Effects of different cross-flow fans on the hovering aerodynamic characteristics of a propulsive wing. *Energy*, *322*, 135559. https://doi.org/10.1016/j.energy.2025.135559

Ma, Y., Wang, C., Han, Z., & Wang, Y. (2025). Mid-fidelity aero-propulsive coupling approach for distributed propulsion aircraft. *Aerospace Science and Technology*, *157*, 109859. https://doi.org/10.1016/j.ast.2024.109859

Nabawi, R. A., Syahri, B., Alfana, Y. D., & Fernandez, D. (2026). Hydrodynamic optimization of a Sweptback Stern Foil for resistance reduction in flat-hull ships: A CFD-based extension of the Hull Vane concept. *Teknomekanik*, *9*(1), 110–120. https://doi.org/10.24036/teknomekanik.v9i1.54872

Nguyen, K., Potnis, A., Saha, A., & Friend, J. (2025, January 6). Enhancing Breakup of Liquid Sheets in Quiescent Air Using MHz-Order Acoustic Waves. *AIAA SCITECH 2025 Forum*. AIAA SCITECH 2025 Forum. https://doi.org/10.2514/6.2025-2164

Numerical Investigation of Swirl Recovery from a Transonic Propeller with Swirl Recovery Vanes. (2025). *Journal of Applied Fluid Mechanics*, *18*(4). https://doi.org/10.47176/jafm.18.6.3136

Oh, H., Li, W., & Ladeinde, F. (2025, January 6). Impact of Multiple Detonation Waves on Heat Flux in Rotating Detonation Engines. *AIAA SCITECH 2025 Forum*. AIAA SCITECH 2025 Forum. https://doi.org/10.2514/6.2025-2316

Riegler, C., Mutter, J., & Kayal, H. (2025). Comparison of autorotation and propulsive landing for planetary exploration. *Acta Astronautica*, *234*, 26–40. https://doi.org/10.1016/j.actaastro.2025.04.008

Shan, X., & Bilgen, O. (2025). Multi-physics finite state fully coupled modeling of mechanism-free induced-strain actuated ornithopters. *Aerospace Science and Technology*, *166*, 110573. https://doi.org/10.1016/j.ast.2025.110573

Shi, W., Tadros, M., Gomez, D., Nurnberg, M., Friedhoff, B., Felli, M., Eslamdoost, A., Aubert, A., & Flori, A. (2025). Development of Energy Efficient Solutions for Hydrogen Powered Vessels: RESHIP Project. In C. McNally, P. Carroll, B. Martinez-Pastor, B. Ghosh, M. Efthymiou, & N. Valantasis-Kanellos (Eds.), *Transport Transitions: Advancing Sustainable and Inclusive Mobility* (pp. 420–425). Springer Nature Switzerland. https://doi.org/10.1007/978-3-031-89444-2_61

Suman, P., Prasad, B. R., Prusty, G., Babu, Ch. M., & Khan, I. (2026). IoT-Enhanced Statistical Methods for Process Optimization in Biotechnology and Pharmaceutical Manufacturing. In K. C. Rath & K. Muduli, *AIoT-Driven Sustainable Manufacturing and Operational Initiatives* (1st ed., pp. 76–94). CRC Press. https://doi.org/10.1201/9781003503323-5

Sun, X., Wang, C., Wang, S., Tian, X., Li, J., & Wang, J. (2025). Fluid-Structure Interaction and Modal Analysis of Hydraulic Turbines. *Journal of Physics: Conference Series*, *3150*(1), 012047. https://doi.org/10.1088/1742-6596/3150/1/012047

Sun, Y., Ge, S., Wu, R., Chen, W., Han, H., Ma, D., & Ping, H. (2026). Numerical prediction on cavitation characteristics of a marine propeller in oblique flow without and with hull wake effects. *Ocean Engineering*, *352*, 124567. https://doi.org/10.1016/j.oceaneng.2026.124567

Tao, H., Shi, G., Zuo, Z., Chen, J., Li, J., & Chen, H. (2026). Study of unsteady aerodynamic loads and structural response of axial flow compressor in compressed air energy storage system. *Energy Sources, Part A: Recovery, Utilization, and Environmental Effects*, *48*(1), 2699335. https://doi.org/10.1080/15567036.2026.2699335

Wang, M., Li, X., & Zhang, S. (2026). A Cascaded trim method of electric aircraft subject to propulsive constraints in wing-borne flight. *Aerospace Science and Technology*, *171*, 111589. https://doi.org/10.1016/j.ast.2025.111589

Wang, X., Zhou, C., Wang, J., Fan, J., Yin, Z., Zhu, C., & Deng, L. (2024). CMBUV: A Composite-Mechanism Bioinspired Underwater Vehicle Integrated With Elasticity and Shear Damping Possesses High-Performance Capability. *IEEE Transactions on Intelligent Vehicles*, *9*(1), 1628–1640. https://doi.org/10.1109/TIV.2023.3286820

Wang, X., Zhou, C., Wang, J., Yin, Z., Shuai, P., & Song, S. (2026). Online Magnetorheological Damping Modulation of a Robotic Tuna for Enhanced Speed and Efficiency. *IEEE/ASME Transactions on Mechatronics*, 1–11. https://doi.org/10.1109/TMECH.2026.3659892

Wei, J., Gao, W., Lu, B., & Li, Q. (2026). Aero-Propulsive-Elastic Coupled Modeling of Distributed Electric Propulsion Systems with Slipstream Interactions. *Aerospace*, *13*(7), 613. https://doi.org/10.3390/aerospace13070613

Yan, C., & Zhang, B. (2026). Initiation and Propulsive Performance of Bump-Induced Oblique Detonation Waves. *AIAA Journal*, *64*(7), 3974–3989. https://doi.org/10.2514/1.J066322

Ye, L., Liu, H., Ding, Q., Hu, Z., Li, W., Cui, W., & Fan, D. (2026). Deep-Sea Biomimetic Manta Ray Robots: A Comprehensive Review Based on Operational Depth Spectrum, Structures, Energy Optimization, and Control Systems. *Biomimetics*, *11*(3), 216. https://doi.org/10.3390/biomimetics11030216

Zeng, H., Fang, T., Xin, J., Jin, Q., Duan, Y., & Wan, L. (2026). Hydrodynamic performance and wake pattern in self-propelled side-by-side fish: Effects of phase difference and lateral spacing. *Ocean Engineering*, *353*, 124830. https://doi.org/10.1016/j.oceaneng.2026.124830

Zhang, T., Liang, Z., Zheng, H., Chen, Z., Zheng, K., Xu, R., Liu, J., Zhu, H., Guan, Y., Xu, K., & Ding, X. (2025). Mole-inspired Forepaw Design and Optimization Based on Resistive Force Theory. *Journal of Bionic Engineering*, *22*(1), 171–180. https://doi.org/10.1007/s42235-024-00633-0

Zhang, X., Gan, Z., Zhang, L., Liu, Z., Liu, S., Chen, Q., Shang, Z., & Duan, Z. (2026). Thrust Performance and Propulsive Efficiency of Bioinspired Piston-Type Synthetic Jet Underwater Propellers. *Journal of Bionic Engineering*, *23*(5), 2853–2866. https://doi.org/10.1007/s42235-026-00939-1

Zhou, R., & Lin, S. (2026). Design of a distributed negative-pressure adsorption robot for energy-efficient closed-loop cleaning based on FSI and multi-physics optimization. *Mechanics & Industry*, *27*, 6. https://doi.org/10.1051/meca/2026003

Zhu, H., Lin, L., Yu, C., Chen, Y., Xiong, H., Xing, Y., & Zheng, G. (2024). The Design and Application of a Vectored Thruster for a Negative Lift-Shaped AUV. *Actuators*, *13*(6), 228. https://doi.org/10.3390/act13060228

Copyright Holder :
© Ardiansyah. (2026).

First Publication Right :
© Journal of Moeslim Research Technik

This article is under: